Grid-Based Variable Speed Wind Energy Conversion System Power Quality Improvement

Boya Vijaykumar[1], P. Pedda Reddy[2], Dr. K. Chithambaraiah Setty[3]

[1]PG Student, Department of Electrical and Electronics Engineering, ST. Johns College of Engineering and Technology, Yerrakota, Yemmiganur, Kurnool, 518360, AP, India.
[2]Assistant Professor, "Department of Electrical and Electronics Engineering, ST. Johns College of Engineering and Technology, Yerrakota, Yemmiganur, Kurnool, 518360, AP,India.
[3]Associate Professor, "Department of Electrical and Electronics Engineering, ST. Johns College of Engineering and Technology, Yerrakota, Yemmiganur, Kurnool, 518360, AP, India.

***Abstract*—** The analysis, design, and management of a variable speed wind energy conversion system (WECS) with a grid-interfaced doubly fed induction generator (DFIG) for power smoothening with maximum power point tracking (MPPT) capabilities are the topics of this study. The rotor position computation technique is used by this DFIG. For supplying regulated electricity to the grid, the grid-side converter's control algorithm is adjusted. To achieve MPPT and unity power factor functioning at the stator terminals, the rotor-side converter is regulated. In order to be suitable for modelling all different induction generator configurations, the entire system has been modelled and simulated in the MATLAB Simulink environment.

I. INTRODUCTION

The output of Earth's fossil fuels, such as coal, gas, and oil, is finite, and it is anticipated that they will be consumed past their peak in the coming decades. As a result, energy costs might continue to grow. Future energy demands can be satisfied by increasing the contribution of renewable energy sources. Because there are no harmful emissions to the environment from renewable sources, they are climate-friendly [1]. Because to developments in power electronics, wind energy is one of the least expensive renewable energy options [2]. Because of their simplicity and low cost, fixed speed wind energy conversion systems (wecss) using squirrel cage induction machines are frequently used. One can plainly see from the wind turbine characteristics that for various wind speeds, the machine should run at various rotor speeds to achieve maximum output. Fixed speed induction generators (FSIG) are less effective since they operate at the same speed regardless of the wind speed [3]. These fixed speed generators draw a significant amount of lagging reactive power because the stator is directly connected to the grid. In order to significantly increase energy output and achieve unity power factor, variable speed induction generators are now used to run at desired speed using power electronic converters [4]. Due to the reduction in the size of the power converters and the converter losses, the double fed induction generator (DFIG) is the most popular variable speed WECS architecture [5]–[7]. Due to its energy yield compared to cost, DFIG with a single-stage gearbox appears to be the most intriguing option [7]. Both the active and reactive powers of DFIG have been successfully controlled using vector control techniques [8], [9]. The fluctuation in power produced by the wind turbine is particularly considerable due to the intermittent nature of wind. When wind energy penetration in the grid rises, this issue becomes more severe. There have been numerous attempts to lessen the unstable impact of wind power generation on the grid [10]–[15]. The fluctuating wind power is smoothed using a variety of methods, including Pref versus m and tip speed ratio (TSR) control [10]. But because it is not functioning at MPPT in this instance, the power yield is decreased. By incorporating energy storage into the WECS, this problem can be solved. For the purpose of enhancing power quality, the performance analysis of various hybrid energy storage systems connected to wind turbines is examined [11]. For various time scales, the operational suitability of various energy storage technologies is compared. [12] also looks into the proper sizing of storage and energy capacity required for a given power rating. Super capacitors are a type of short-term energy storage device that is used to smooth out fast wind-induced power variations [13], [14]. In [15], Li-ion capacitors are suggested as a viable remedy for power fluctuation filtering at the range of tens of seconds. Integrating a flywheel with a DFIG allows for the smoothing of power fluctuations and voltage fluctuations. As a result, the penetration of wind energy in the grid rises. For a time scale of 20 minutes, flywheel storage is typically preferred, though [10].

The grid interfaced DFIG based WECS is the power smoothing solution proposed in this paper. The rotor position is estimated using the rotor position computation algorithm (RPCA). The work's control of

the grid side converter is new (GSC). The control algorithm for supplying regulated electricity to the grid has thus been demonstrated by the authors in a transparent manner. The second crucial element of DFIG-based WECS for power smoothening is the use of BESS. By contrasting the traditional and suggested DFIGs, it is possible to see how the powers change as wind speeds increase. The system's functionality for controlling the power of DFIG even with changeable wind speed circumstances has been experimentally proven.

II SYSTEM CONFIGURATION AND CONTROL PRINCIPLE

Fig. 1 depicts the conceptual diagram of the proposed grid-interfaced, DFIG-based WECS. Two VSCs that are linked back to back share a DC link with BESS. Here, the stator and grid are joined directly. RSC is managed in a reference frame that is voltage-oriented. Using an augmented phase locked loop, the d-axis of the synchronously rotating reference frame is aligned with the voltage axis (EPLL). The position estimate in this case uses the rotor position computation technique. The GSC is managed such that the grid receives the regulated electricity. When the amount of electricity generated exceeds the regulated amount, the excess power is stored in the BESS. The BESS feeds the residual electricity to the grid if the amount of power generated falls short of the regulated amount. In Fig. 2, the control algorithms are displayed.

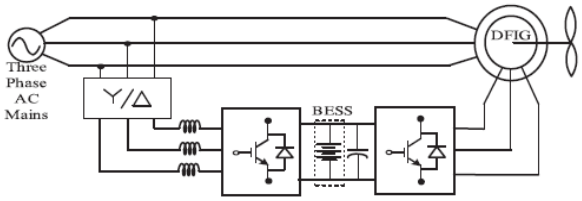

Fig. 1. Proposed system configuration.

III CONTROL STRATEGY

A. Control Algorithm

In this Section, control methods for sensor-free functioning of DFIG, GSC, and RSC are covered in depth. Figure 2 displays a conceptual control diagram for the GSC and RSC. The RSC is able to independently control both active and reactive capabilities. The operational maximum power point is attained with this RSC control. RSC is managed in a reference frame that is voltage-oriented. Therefore, the d and q axis rotor reference currents (Idr and Iqr) govern the active and reactive powers, respectively. The speed error (er) between the reference and estimated rotor speeds (- r and r) is processed as follows to produce the direct axis rotor reference current (I*dr) using a proportional integral (PI) speed controller.

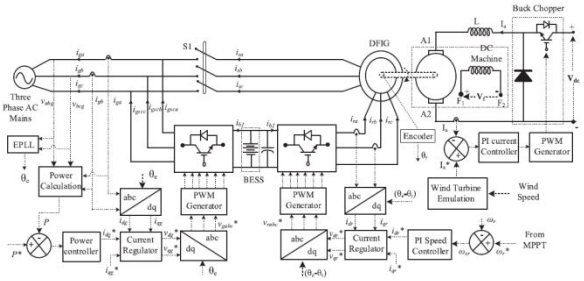

Fig. 2. Control algorithm of the proposed WECS

$$I^*_{\mathrm{dr}}(n) = I^*_{\mathrm{dr}}(n-1) + k_{\mathrm{pd}}\left[\omega_{\mathrm{er}}(n) - \omega_{\mathrm{er}}(n-1)\right] + k_{\mathrm{id}}\,\omega_{\mathrm{er}}(n)$$

Where *k*pd, *k*id are the proportional and integral gains of speed controller. ωer(n) and ωer(n − 1) are the speed errors at nth and (n − 1)th instant. I^* dr(n) and I^* dr(n − 1) are the direct axis rotor reference currents at nth and (n − 1)*th* instant. The rotor speed (ωr) of the DFIG is estimated using RPCA sensorless algorithm. Reference speed (ω-*r*) is selected for achieving MPPT. In this algorithm, the reference rotor speed is estimated using TSR control using wind speed. The reference quadrature axis rotor current (*I**qr) is selected to control the reactive power to zero at stator terminals. The direct and quadrature axis rotor currents (*I*dr and *I*qr) are computed from sensed rotor currents (*i*ra, *i*rb and *i*rc) as

$$I_{\mathrm{dr}} = \frac{2}{3}\left[i_{\mathrm{ra}}\sin\theta_{\mathrm{slip}} + i_{\mathrm{rb}}\sin\left(\theta_{\mathrm{slip}} - \tfrac{2\pi}{3}\right) + i_{\mathrm{rc}}\sin\left(\theta_{\mathrm{slip}} + \tfrac{2\pi}{3}\right)\right]$$

$$I_{\mathrm{qr}} = \frac{2}{3}\left[i_{\mathrm{ra}}\cos\theta_{\mathrm{slip}} + i_{\mathrm{rb}}\cos\left(\theta_{\mathrm{slip}} - \tfrac{2\pi}{3}\right) + i_{\mathrm{rc}}\cos\left(\theta_{\mathrm{slip}} + \tfrac{2\pi}{3}\right)\right]$$

where slip angle (θslip) is calculated as

$$\theta_{\mathrm{slip}} = \theta_e - \theta_r.$$

According to Fig. 3, the voltage angle e is computed using EPLL. The RPCA sensorless technique is used to determine the rotor position (r). Two current controllers are used to control the direct and quadrature axis rotor currents (Idr and Iqr) in close proximity to the reference direct and quadrature axis rotor currents (I*dr and I*qr).

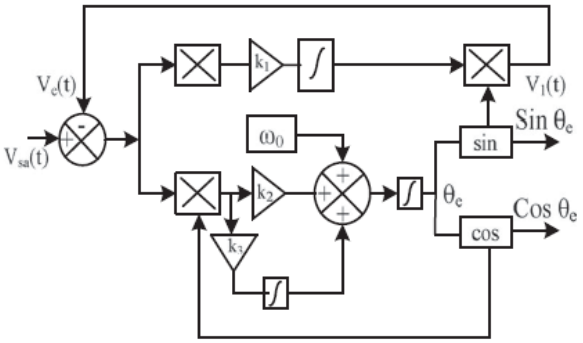

Fig. 3. Enhanced phase locked loop

B. Control of GSC

The control of GSC is what makes this piece unique. This GSC's control is carried out using a reference frame that is voltage-oriented. The direct and quadrature grid currents (Idg & Iqg) are used to regulate the active and reactive powers (P & Q) provided to the grid, respectively. The reference power (P*) is used to get the direct axis grid current (Idg) as

$$I^*_{\mathrm{dg}} = \left(\frac{2}{3}\right)\left(P^*/V_{\mathrm{dg}}\right).$$

I* qg is chosen to be zero in order to achieve unity power factor at the ac mains. The detected grid currents are used to estimate the actual direct and quadrature grid currents (Idg and Iqg). A PI controller processes the error (Ideg and Iqeg) between the actual direct and quadrature currents (Idg and Iqg) and the reference currents (I*dg and I*qg), as indicated as,

$$V'_{\mathrm{dg}}(n) = V'_{\mathrm{dg}}(n-1) + k_{\mathrm{pdv}}\left\{I_{\mathrm{deg}}(n) - I_{\mathrm{deg}}(n-1)\right\} + k_{\mathrm{idv}}\, I_{\mathrm{deg}}(n)$$

$$V'_{\mathrm{qg}}(n) = V'_{\mathrm{qg}}(n-1) + k_{\mathrm{pqv}}\left\{I_{\mathrm{qeg}}(n) - I_{\mathrm{qeg}}(n-1)\right\} + k_{\mathrm{iqv}}\, I_{\mathrm{qeg}}(n)$$

Where *k*pdv, *k*idv are the proportional and integral gains of direct axis current controller. *k*pqv, *k*iqv are proportional and integral gains of quadrature axis current controller. *I*deg (*n*) and *I*deg (*n* − 1) are direct axis current errors at nth and (*n* − 1)*th* instant. *V* _ dg (*n*) and *V* _ dg (*n* − 1) are the direct axis grid voltages at nth and (*n* − 1)*th* instant. *I*qeg (*n*) and *I*qeg (*n* − 1) are the quadrature axis grid current errors at nth and (*n* − 1)*th* instant. *V* _ qg (*n*) and *V* _ qg (*n* − 1) are the quadrature axis grid voltages at nth and (*n* − 1)*th* instant. Direct and quadrature axis grid voltages (*V* _ dg and *V* _ qg) are added with the compensation terms for achieving reference direct and quadrature axis grid voltages (*V**dg and *V**qg). Three phase reference grid voltages (*v**ga, *v**gb, *v**gc) are calculated from the reference direct and quadrature voltages (*V**dg, *V** qg). These reference grid voltages (*v**ga, *v**gb, *v** c) are compared with PWM signals and then these pulses are fed to the GSC.

C. Rotor Position Computation Algorithm

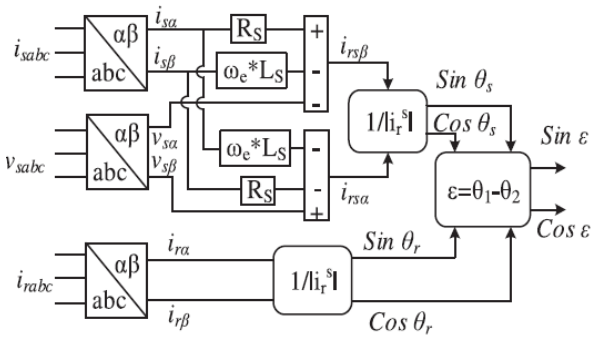

Fig. 4. Rotor position computation algorithm

$$\cos\,\theta_r = \frac{i_{r\alpha}}{\sqrt{i^2_{r\alpha} + i^2_{r\beta}}}$$

$$\sin\,\theta_r = \frac{i_{r\beta}}{\sqrt{i^2_{r\alpha} + i^2_{r\beta}}}.$$

In this algorithm, rotor current (*ir*) makes an angle *θ*s from the stator co-ordinate system and the same rotor current (*ir*) makes an angle *θ*r from the rotor co-ordinate system. The angle between stator and rotor is calculated as (*θm*)est= (*θs* −*θr*). The schematic diagram of sensorless scheme is shown in Fig. 4. Rotor currents (*i*ra, *i*rb) are sensed and transformed into two phases using Clarke's transformation (*irα* &*irβ*).

RESULTS AND DISCUSSION

The steady state and dynamic behaviors of regulated power DFIG based WECS is presented in this section. Simulation results are recorded in terms of line voltage (*v*ab), grid currents (*i*ga,*i*gb and *igc*), stator currents (*i*sa ,*i*sb and *i*sc), GSC currents (*i*GSCa,*i*GSCb and *i*GSCc), rotor currents (*i*ra ,*i*rb and *i*rc), stator power (*PS*), grid power (*PG*), GSC power (*P*GSC), battery voltage (*Vb*), battery current (*Ib*), quadrature axis rotor current (*I*qr), direct axis rotor current (*I*dr), quadrature axis reference rotor current (*I**qr), direct axis reference rotor current (*I**dr), rotor speed (*ω*r), reference rotor speed (*ω* - *r*) and wind speed (*vw*). The power that is discharging from the battery through GSC and RSC are considered as positive. Conversely, the battery charging is taken as negative through both GSC and RSC.

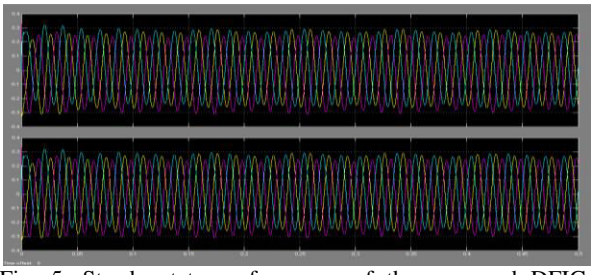

Fig. 5. Steady state performance of the proposed DFIG based WECS at fixed wind speed of 7 m/sec

The simulation results of the suggested DFIG-based WECS are shown in Fig. 5 for a fixed wind speed of 7 m/s. The reference rotor speed is chosen to be 0.7 p.u. to get the wind turbine to produce as much electricity as possible. The PG, PS, and PGSC are depicted in Fig. 5. These findings show that, as a result of the low wind speed, the grid power is maintained at 1.25 kW and the stator power is 0.86 kW. Therefore, the battery is the source of any residual power, as seen in Fig.

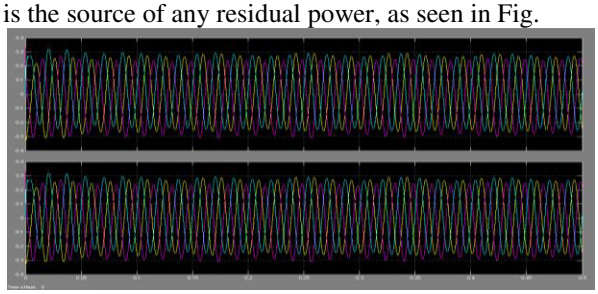

Fig: 6 Stator Power (*PS*)

Fig. 6 displays the simulation results of the proposed WECS at a fixed wind speed of 8.5 m/s. For MPPT operation, a reference rotor speed of 0.86 p.u. is chosen. As shown in Fig. 6, the power feeding to the grid is maintained at 1.25 kW despite varying wind speeds.

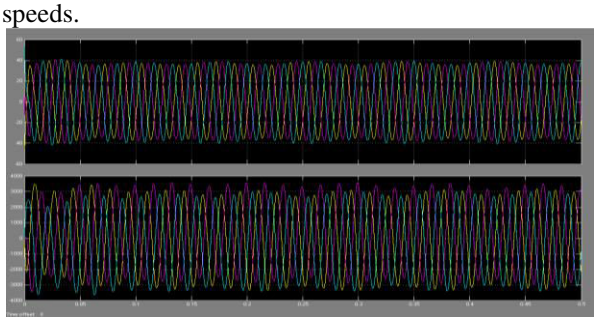

Fig: 7 GSC Power (PGSC).

However, as seen in Fig. 6, the stator power is 1.41 kW. As seen in Fig. 6, the GSC will charge the battery using the remaining power.

Fig. 7 displays the simulation results with a fixed wind speed of 9.15 m/s (1500 rpm). According to MPPT, 1500 rpm is chosen as the reference speed (* r). As seen in Fig. 7, the grid power is kept at 1.25 kW in this instance as well. Due to the stator's output exceeding the reference power command and the battery's GSC-enabled charging, as seen in Figure 7,

Fig. 8 illustrates the sensorless algorithm's efficiency at various rotor speeds. Where sin (r), sin (s), and sin (m) are unit vectors of rotor position angle, unit templates of rotor currents aligned to stator axis, and unit templates of rotor currents aligned to rotor axis, respectively.

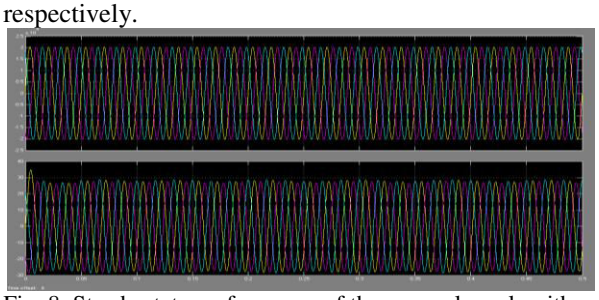

Fig. 8. Steady state performance of the sensor less algorithm of constant power DFIG

CONCLUSION

By adding BESS to the DC connection, it has been discovered that the proposed DFIG-based WECS is capable of delivering regulated power at all wind speeds. In this DFIG-based WECS, the BESS design has been detailed in full. For the purpose of supplying the grid with controlled power, the GSC control algorithm has been updated. The simulation results for both fixed and variable wind speeds at all conceivable rotor speeds have been used to validate the performance of the proposed DFIG. Through the use of simulation data, the suggested DFIG's good dynamic performance has been established. Even at lower wind speeds, this suggested WECS has been demonstrated to be favourable for delivering electricity. With this suggested DFIG, power requirements can be met, even temporarily.

REFERENCES

[1] Manfred Stiebler, *Wind Energy Systems for Electric Power Generation*. New York, NY, USA: Springer-Verlag, 2008.

[2] H.-J.Wagner and J. Mathur, *Introduction to Wind Energy Systems Basics, Technology and Operation*. New York, NY, USA: Springer-Verlag, 2009.

[3] S. S.Murthy, B. Singh, P. K. Goel, and S. K. Tiwari, "A comparative study of fixed speed and variable speed wind energy conversion systems feeding the grid," in *Proc. IEEE 7th Int. Conf. Power Electron. Drive Syst.*, Nov. 27–30, 2007, pp. 736–743.

[4] M.Mansour,M. N.Mansouri, andM. F. Mimouni, "Comparative study of fixed speed and variable speed wind generator with pitch angle control," in *Proc. Int. Conf. Commun., Comput. Control Appl.*, Mar. 3–5, 2011, pp. 1–7.

[5] R. Datta and V. T. Ranganathan, "Variable-speed wind power generation using doubly fed wound rotor induction machine-a comparison with alternative schemes," *IEEE Trans. Energy Convers.*, vol. 17, no. 3, pp. 414–421, Sep. 2002.

[6] L. Holdsworth, X. G. Wu, J. B. Ekanayake, and N. Jenkins, "Comparison of fixed speed and doubly-fed

induction wind turbines during power system disturbances," *IEE Proc. Gener., Transmiss. Distrib.*, vol. 150, no. 3, pp. 343–352, 2003.
[7] H. Polinder, F. F. A. Van Der Pijl, G. J. de Vilder, and P. J. Tavner, "Comparison of direct-drive and geared generator concepts for wind turbines," *IEEE Trans. Energy Convers.*, vol. 21, no. 3, pp. 725–733, May 2005.
[8] S. Muller, M. Deicke, and R. W. De Doncker, "Doubly fed induction generator systems for wind turbines," *IEEE Ind. Appl. Mag.*, vol. 8, no. 3, pp. 26–33, May/Jun. 2002.
[9] R. Pena, J. C. Clare, and G. M Asher, "Doubly fed induction generator using back-to-back PWM converters and its application to variable speed wind-energy generation," *Proc. Elect. Power Appl.*, vol. 143, no. 3, pp. 231–241, May 1996.
[10] C. Luo, H. Banakar, B. Shen, and B.-T. Ooi, "Strategies to smooth wind power fluctuations of wind turbine generator," *IEEE Trans. Energy Convers.*, vol. 22, no. 2, pp. 341–349, Jun. 2007.
[11] Y. Kim and R. Harrington, "Analysis of various energy storage systems for variable speed wind turbines," in *Proc. IEEE Conf. Technol. Sustain.* Ogden, UT, USA, 2015, pp. 7–14.
[12] J. P. Barton and D. G. Infield, "Energy storage and its use with intermittent renewable energy," *IEEE Trans. Energy Convers.*, vol. 19, no. 2, pp. 441–448, Jun. 2004.
[13] C. Abbey and G. Joos, "Super capacitor energy storage forwind energy applications," *IEEE Trans. Ind. Appl.*, vol. 43, no. 3, pp. 769–776, May/Jun. 2007.
[14] L. Qu and W. Qiao, "Constant power control of DFIG wind turbines with super capacitor energy storage," *IEEE Trans. Ind. Appl.*, vol. 47, no. 1, pp. 359–367, Jan./Feb. 2011.
[15] G. Mandic, A. Nasiri, E. Ghotbi, and E. Muljadi, "Lithium-Ion capacitor energy storage integrated with variable speed wind turbines for power smoothing," *IEEE J. Emerg. Sel. Topics Power Electron.*, vol. 1, no. 4, pp. 287–295, Dec. 2013.
[16] R. Cardenas, R. Pena, G. Asher, and J. Clare, "Power smoothing in wind generation systems using a sensorless vector controlled induction Machine driving a flywheel," *IEEE Trans. Energy Convers.*, vol. 19, no. 1, pp. 206–216, Mar. 2004.
[17] S. Ghosh and S. Kamalasadan, "An energy function-based optimal control strategy for output stabilization of integrated DFIG-Flywheel energy storage system," *IEEE Trans. on Smart Grid*, vol. PP, no. 99, pp.1–10, to be published.
[18] D. H. Doughty, P. C. Butler, A. A. Akhil, N. H. Clark, and J. D. Boyes, "Batteries for large-scale stationary electrical energy storage," in *Proc. Electrochem. Soc. Interface*, Fall 2010, pp. 49–53.